Th A3 07

Towards High Resolution Localised Elastic Full Waveform Inversion

S. Yuan* (Institut de Physique du Globe de Paris), N. Fuji (Institut de Physique du Globe de Paris), S. Singh (Institut de Physique du Globe de Paris), D. Borisov (Princeton University)

Summary

We present a methodology to invert seismic data for a localised area by combining source-side wavefield injection and receiver-side extrapolation method. Despite the high resolving power of seismic full waveform inversion (FWI), the computational cost for practical scale elastic FWI remains a heavy burden. This can be much more severe for time-lapse surveys, which require real-time seismic imaging on a daily or weekly basis. Besides, structure changes during time-lapse surveys are likely to occur in a small area rather than the whole region, such as oil reservoir. We thus propose an approach that allows to image effectively the localised structure changes far deep from both source and receiver arrays. We perform both forward and back propagation only inside the target region. We present 2D elastic numerical examples of the proposed method and quantitatively evaluate the inversion errors, in comparison to those of conventional full-model inversions. The results show that the proposed localised waveform inversion is not only efficient and robust but also accurate even under the existence of errors in baseline models. Besides, the proposed strategy has the potentiality in determining high-resolution imaging of reservoir by inverting higher frequencies (above 30 Hz) at relatively low computational cost.

Introduction

Amongst many proposed tomography methodologies in seismology, full waveform inversion has emerged as one of the most promising and powerful techniques since over three decades ago (e.g. Virieux and Operto, 2009). However, waveform inversion requires repeated full wavefield modellings and it is thus computationally expensive to invert for a large area. Computational problem can be particularly more severe for time-lapse surveys in exploration seismology, which require real-time model estimations on a regular basis (daily or weekly). Since the oil/gas production does not change the overall substructures, there should be much redundancy in conventional full-model waveform inversions. In this study, we propose a methodology that allows to locally perform waveform inversions in the region disconnected from both source and receiver arrays.

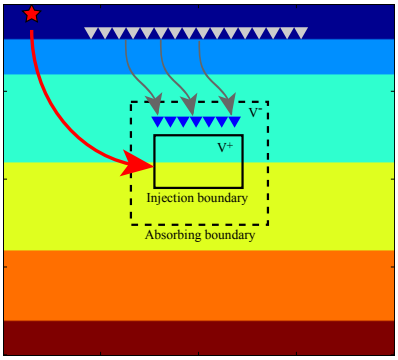


Figure 1 *An schematic illustration of the proposed localised inversion in a layered model. Red star denotes the physical source. Grey and blue triangles denote physical and virtual receivers, respectively. The Dashed square represents the absorbing boundary and the solid square represents the source injection boundary.*

Fig. 1 shows how our methodology works. We have a physical source (array) and a receiver array on the Earth's surface or ocean bottom. Instead of performing inversion inside the whole model region, we would like to focus on a subvolume in V^+, where the model changes are expected to occur. All forward and backward simulations will be conducted within the reduced absorbing boundary (the dashed square shown in Fig. 1). Such a strategy of localised waveform inversion requires two levels of wavefield reconstructions: i) representation of seismic sources in the subdomain (wavefield injection method); and ii) extrapolation of residual wavefield between baseline and monitor surveys recorded at the physical receivers to virtual receivers in the subdomain (residual wavefield extrapolation). Borisov et al. (2015) proposed a localised waveform inversion technique for time-lapse surveys within a target region disconnected from source arrays. However, there are few studies that extended it to a region disconnected both from source and receiver arrays. To demonstrate the feasibility, efficiency and robustness of the proposed methodology, we perform a series of 2D elastic numerical examples in comparison to those of conventional full-model inversions. Furthermore, we also show the potentiality in determining high-resolution imaging of reservoir by inverting higher frequencies (above 30 Hz) at relatively low computational cost.

Method - Wavefield injection and extrapolation

For the source side, wavefield injection method (Robertsson and Chapman, 2000) reconstructs a source expression on the surface of target regions, which serves as a localised forward modelling scheme and allows efficient calculation of synthetic seismograms after model alterations within a target area. Wavefield injection is essentially a hybrid approach, where we impose an artificial boundary to divide the whole computational domain into two subdomains V^+ and V^- (Fig 1). Given a model of the full region, we can pre-calculate wavefield from the source outside the target region to the source injection boundary (Fig. 1, solid square) and store them. The stored wavefield will serve as a new source distribution (boundary condition) for subsequent localised forward modelling. The only missing part of the wavefield from injection method is the interactions of the scattered wavefield caused by the altered model within target area (Fig. 1, solid square) with the unaltered model outside the reduced absorbing

boundary (Fig. 1, dashed square). However, we will show, in following numerical examples, that these higher-order, long-range interactions may impose limited effect on the final inversion results.

For the receiver side, extrapolation of wavefield from physical to virtual receivers in the subsurface is needed in our methods to perform localised waveform inversion. We extrapolate residual wavefield between baseline and monitor in frequency domain using correlation-type representation theorem (Wapenaar and Fokkema, 2006):

$$u_n^1(\mathbf{r}_A) \quad \sim \quad \int_{S'} dSn_j[G_{in}^{0*}(\mathbf{r},\mathbf{r}_A)C_{ijkl}^0 u_{k,l}^1(\mathbf{r}) - u_i^1(\mathbf{r})C_{ijkl}^{0*}G_{kn,l}^{0*}(\mathbf{r},\mathbf{r}_A)] \tag{1}$$

where S' denotes the surface covered by the physical receiver array. $u_n^1(\mathbf{r})$ is the i-th component of perturbed displacement at $\mathbf{r}$, n_j denotes the normal vector, $G_{in}^0(\mathbf{r},\mathbf{r}_A)$ denotes the i-th component of Green function from n-th single force at $\mathbf{r}_A$ to $\mathbf{r}$ for baseline model (the asterisk denotes complex conjugate), whereas C_{ijkl}^0 are elastic moduli for the baseline model. The Green's functions $G_{in}^{0*}(\mathbf{r},\mathbf{r}_A)$ between physical and virtual receivers, serving as back-propagators are calculated and stored just once using the baseline model. The truncated integral due to the limited physical receiver geometry in eq. 1 will lead to some spurious events in the extrapolated wavefield (the single-sided illumination problem). As we will show in the later examples, receiver-side wavefield extrapolation combining with source-side wavefield injection can naturally neglect these non-physical extrapolated events.

Numerical examples

We validate our localised inversion strategy on the modified Marmousi model in comparison to full-model inversions. The V_p model is 7.5 km $\times$ 2.5 km (Fig. 2a). V_s ($V_s \approx V_p/1.5 + 300$ m/s) and density models are linearly linked to the V_p model. We generate 4 s of data recorded by ocean bottom acquisitions at 300 m depth with a regular spacing of 25 m. In total 271 receivers record three components of velocity wavefield plus one component of pressure wavefield. A Ricker wavelet with dominant frequency of 6.5 Hz is used as the source wavelet and added onto the vertical velocity component. The grid spacing for the wave propagation is 25 m and the time step is 2 ms. 55 sources are deployed at 275 m depth with the interval of 125 m. The time-lapse velocity perturbations are about 5 % of the average baseline model (Fig. 2b).

The 2D V_p perturbations obtained from full-model and localised inversions under true baseline model are shown in Fig. 2c-d, respectively. Compared to the conventional full-model inversion, the localised inversion retrieves the velocity anomalies with a higher accuracy after the same 100 iterations. The corresponding 1D velocity profiles are shown in Fig. 2. Fig. 3 shows the vertical velocity components of initial and final residuals from one shot gather. The residuals of the major events are better fitted by the localised inversion (Fig. 3d) in comparison to the final full-model inversion residuals (Fig. 3b). We specially plot the theoretical initial residuals (Fig. 3e) in case that we directly record wavefield at the same positions as the extrapolated virtual receivers. The residual difference between Fig. 3c and e is shown in Fig. 3f. This difference essentially represents the spurious events after wavefield extrapolation. We notice that the localised inversion does not "see" those spurious events when comparing it with final residuals of the localised inversion (Fig. 3d).

To acknowledge the fact that no precise information on the interfaces and medium parameters is available, the boundary data for wavefield injection and the Green's functions for wavefield extrapolation should be modelled in a more realistic baseline model. Therefore, we divide inversions into two parts in the second experiment: (a) baseline model inversion (b) time-lapse model inversion. Starting from a smoothed model (Fig. 4b), the baseline models of V_p and V_s are inverted (Fig. 4c, here only V_s model is shown) using lower frequency data, which mainly determines the long wavelength structures. In order to achieve the high-resolution image of target regions, we need to interpolate the obtained baseline model and perform once again a number of full-model forward modelling, so that we can store the high frequency injection boundary wavefield and Green's functions without numerical dispersion. As is shown in Fig 4e and f, higher resolution is achieved at relatively low computational cost due to the reduced modelling regions.

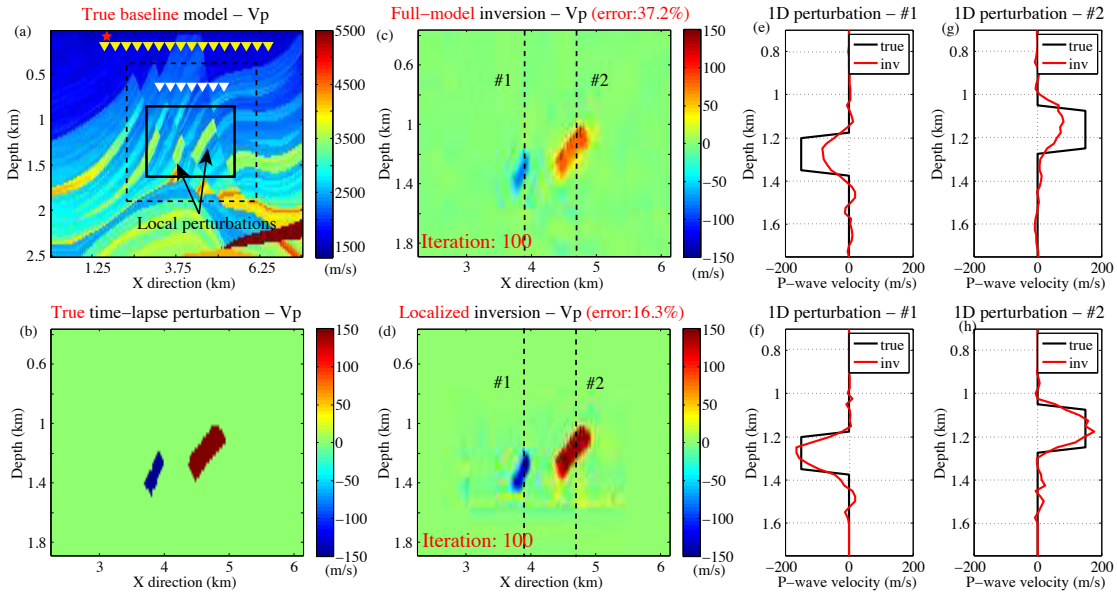


Figure 2 *Time-lapse V_p model and inverted results. (a) The baseline V_p model selected from the true Marmousi model and the acquisition geometry. Red star and yellow triangles denote physical source and receivers, respectively. White triangles denote the extrapolated virtual receivers. Two arrows point to the locations where time-lapse perturbation occurs. (b) The zooming true time-lapse V_p perturbations within the dashed square in (a). (c) Full-model inversion result. (d) Localized inversion result. The 1D true and inverted velocity perturbations (#1 and #2) in (c) and (d) are shown in (e, g) and (f, h), respectively.*

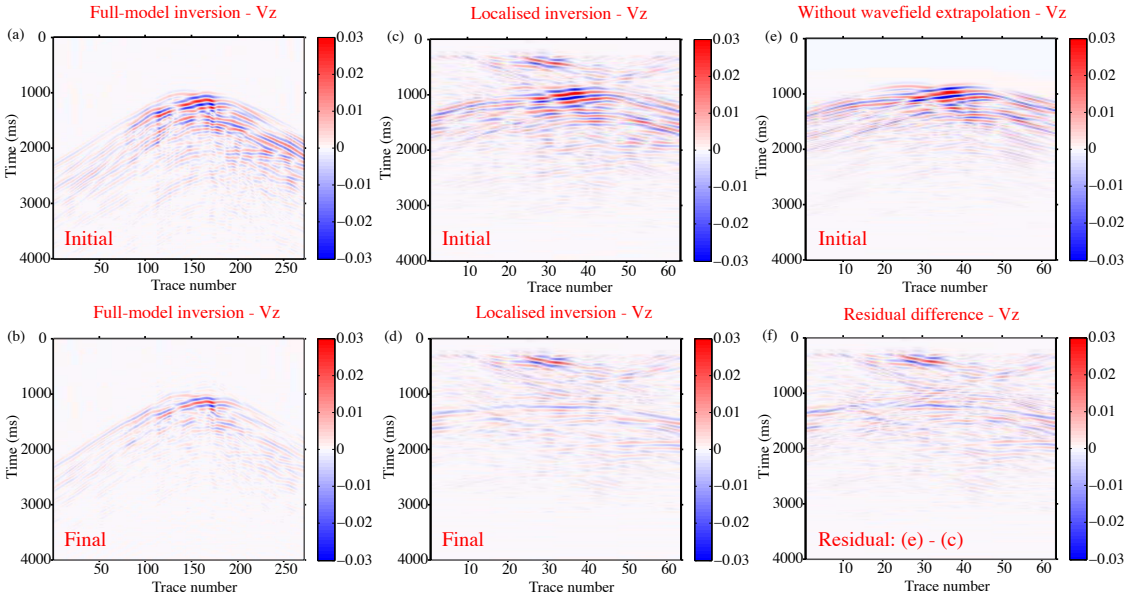


Figure 3 *Vertical component of inversion residuals from one shot example under true baseline Marmousi model. (a-b) Initial and final (after 100 iterations) residuals using full-model inversion. (c-d) Initial and final (after 100 iterations) residuals using localised inversion. (e) Initial residuals of localised inversion using the true wavefield directly observed at virtual receiver positions without extrapolation. (f) The residual difference between (c) and (e).*

Conclusion

We combine wavefield injection and extrapolation to perform the localised waveform inversion for time-lapse seismic surveys. It shows that the localised inversion can enhance the image quality of local time-

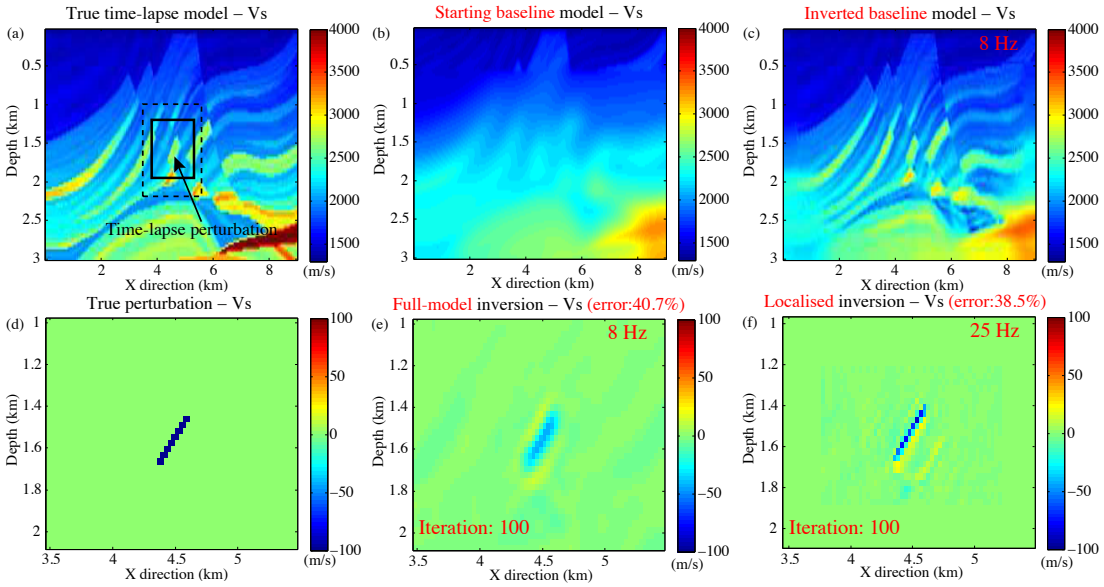


Figure 4 *(a) True V_s baseline model. (b) Starting Vs model for baseline survey. (c) Inverted V_s baseline model. (d) True time-lapse V_s perturbation. (e) Inverted V_s perturbation from full-model inversion with lower frequency contents (8 Hz). (f) Inverted perturbation from localised inversion with higher frequency contents (25 Hz).*

lapse variation while reducing the computational cost to a large extent. The proposed strategy reveals that putting virtual sources and receivers in the vicinity of target region contribute to improving the accuracy and robustness of waveform inversion even under uncertainties of the outside area. It is as if we observed through a telescope to make the distant objects look closer and thus more clearly, even without knowing what is happening between them and us.

Due to the reduced modelling size, the computing time of the 2D localised inversion in the first experiment is approximately decreased by a factor of 10 as compared to full-model inversions. We expect that the severe computational cost of 3D elastic or visco-elastic full waveform inversion during practical time-lapse surveys, could be potentially reduced to a more acceptable and economic level. Although the proposed methodology is examined on 2D cases, the extension to general 3D cases is straightforward.

Acknowledgements

The study was carried out as a part of the Paris Exploration Geophysics Group project (GPX) funded by the French National Research Agency (ANR), CGG, TOTAL and Schlumberger. A significant part of the calculations in this work was performed on S-CAPAD at Institut de Physique du Globe de Paris.

References

Borisov, D., Singh, S.C. and Fuji, N. [2015] An efficient method of 3-D elastic full waveform inversion using a finite-difference injection method for time-lapse imaging. *Geophysical Journal International*, **202**(3), 1908–1922.

Robertsson, J.O. and Chapman, C.H. [2000] An efficient method for calculating finite-difference seismograms after model alterations. *Geophysics*, **65**(3), 907–918.

Virieux, J. and Operto, S. [2009] An overview of full-waveform inversion in exploration geophysics. *Geophysics*, **74**(6), WCC1–WCC26.

Wapenaar, K. and Fokkema, J. [2006] Green's function representations for seismic interferometry. *Geophysics*, **71**(4), SI33–SI46.